International Journal of Nanomedicine

Dovepress
open access to scientific and medical research

Open Access Full Text Article

ORIGINAL RESEARCH

Synovitis in mice with inflammatory arthritis monitored with quantitative analysis of dynamic contrast-enhanced NIR fluorescence imaging using iRGD-targeted liposomes as fluorescence probes

This article was published in the following Dove Press journal:
International Journal of Nanomedicine

Hao Wu[1,2,*]
Haohan Wu[1,2,*]
Yanni He[1]
Zhen Gan[2]
Zhili Xu[1,2]
Meijun Zhou[1,2]
Sai Liu[1,2]
Hongmei Liu[1]

[1]Department of Ultrasonography, Guangdong Second Provincial General Hospital Affiliated to Southern Medical University, Guangzhou, China; [2]Department of Ultrasonography, The Third Affiliated Hospital of Southern Medical University, Guangzhou, China

*These authors contributed equally to this work

Background: Rheumatoid arthritis (RA) is a common inflammatory disorder characterized primarily by synovitis and pannus formation in multiple joints, causing joints destruction and irreversible disability in most cases. Early diagnosis and effective therapy monitoring of RA are of importance for achieving the favorable prognosis.

Methods: We first prepared the targeted fluorescence probes, and then explored the feasibility of near-infrared (NIR) fluorescence molecular imaging to detect and evaluate the RA via the targeted fluorescence probes by quantitative analysis in this study.

Results: The targeted fluorescence probes (indocyanine green-liposomes decorated with iRGD peptide [iLPs]) was successfully prepared. The quantitative analysis found that strong fluorescence signal was detected in inflamed paws and the fluorescence signal in iLPs group was 3.03-fold higher than that in non-targeted (indocyanine green-liposomes decorated without iRGD peptide [LPs]) group ($P<0.01$) at 15 min after injection, whereas the fluorescence signal from iLPs signal can almost not be observed in the non-inflamed paws, showing the high sensitivity and accuracy for arthritis by the NIR fluorescence imaging based on iLPs.

Conclusion: The NIR fluorescence imaging by iLPs may facilitate improved arthritis diagnosis and early assessment of the disease progression by providing an in vivo characterization of angiogenesis in inflammatory joint diseases.

Keywords: rheumatoid arthritis, synovitis, diagnosis, near-infrared fluorescence imaging, iRGD-targeted probes

Introduction

Rheumatoid arthritis (RA) is a common inflammatory disorder characterized primarily by synovitis and pannus formation in multiple joints, causing joint destruction and irreversible disability in most cases.[1] The early diagnosis and aggressive management could greatly favor to treat the disease and to improve the clinical prognosis of RA.[2] Therefore, it is of uttermost importance in RA to recognize early synovitis and to monitor treatment efficacy of inflammatory arthritis.

In the clinical practice, medical imaging is an important tool and has become the mainstay of diagnosis and treatment monitoring. But various conventional imaging modalities are limited by their disadvantages. Radiographic examination that mainly relies on the presence of relatively late features, such as bone erosion and joint space narrowing, has poor sensitivity in early stages of disease.[3,4] Ultrasonography and

Correspondence: Hongmei Liu
Department of Ultrasonography, Guangdong Second Provincial General Hospital Affiliated to Southern Medical University, Courtyard No. 466, Middle Xingang Road, Haizhu District, Guangzhou 510317, China
Tel +86 20 8916 9173
Email hongmeiliu3@163.com

submit your manuscript | www.dovepress.com
Dovepress
http://dx.doi.org/10.2147/IJN.S155475

magnetic resonance imaging (MRI) have been found to have advantages over traditional radiography in terms of sensitivity, but these techniques can only provide anatomical information of established RA.[5–7] However, the use of these techniques is restricted as they are time consuming, highly examiner dependent, of high cost, and have limited availability, thus becoming an obstacle for fast and dynamic assessment of joint inflammation. Recently, there has been a growing demand for more rapid and sensitive tools to detect early synovitis and to monitor the response to therapy.

Near-infrared (NIR) fluorescence imaging is a novel imaging modality that is nonionizing and allows for fast image acquisition times. Also, it has the relatively low tissue absorption, scatter, and minimal auto-fluorescence at the NIR window of 650–900 nm. Meanwhile, through constructing the targeted probes, it can achieve sensitive and selected detection of biologic processes at the cellular and molecular levels, displaying significant potential to provide noninvasive molecular imaging for disease diagnosis.[8,9]

Integrin αvβ3, a well-known angiogenesis marker, is overexpressed in the activated endothelial cells (ECs) or during angiogenesis.[10,11] Studies showed angiogenesis is an early event in the inflammatory joint, enabling activated monocytes to enter the synovium and expanding it into a pannus via ECs by active recruitment.[12–14] Moreover, Storgard et al demonstrated that using a αvβ3 integrin inhibitor during angiogenesis blockade in arthritis can decrease synovial inflammation and increase EC apoptosis, thus ultimately disrupting the progression of RA in preventative dosing regimens.[15] Therefore, in the present study, we first prepared the αvβ3-targeted fluorescence probes, and then explored the feasibility of NIR fluorescence molecular imaging to detect and evaluate the RA via αvβ3-targeted fluorescence probes.

Materials and methods

Materials

1,2-Distearoyl-sn-glycero-3-pho-sphoethanolamine-N-[met-hoxy(poly-ethyleneglycol)-2000] (DSPE-PEG_{2000}), 1,2-distearoyl-sn-glycero-3phosphoethanolamine-N-[maleimide(polyethylenegl-ycol)-2000] (DSPE-PEG_{2000}-Mal), dipalmitoylphosphatidylcholine (DPPC), and cholesterol were purchased from Avanti Polar Lipids Inc (Alabaster, AL, USA). iRGD peptide (CRGDKGPDC) was synthesized by GL biochem Ltd (Shanghai, China). Indocyanine green (ICG) and tumor necrosis factor alpha (TNF-α) were purchased from Sigma-Aldrich Co. (St Louis, MO, USA). Bovine type II collagen, complete Freund's adjuvant, and incomplete Freund's adjuvant were purchased from Condrex, Redmond, WA, USA. Human umbilical vein endothelial cells (HUVECs) were purchased from the American Type Culture Collection (Manassas, VA, USA). Male DAB/1J mice were obtained from Vitalriver Experimental Animal Technology Ltd (Beijing, China). Animals received care in accordance with the Guidance Suggestions for the Care and Use of Laboratory Animals.

Preparation and characterization of targeted probes

Firstly, DSPE-PEG_{2000}-iRGD was synthesized through a reaction between DSPE-PEG_{2000}-Mal and iRGD. Then, DPPC, cholesterol, DSPE-PEG_{2000}, and DSPE-PEG_{2000}-iRGD were dissolved in chloroform in a 55:40:4:1 molecular ratios, and later ICG was also added to the mixture of phospholipids. The mixture was then dried under N_2 gas and reduced pressure into a thin film, followed by vacuum desiccation for 3 h at room temperature according to our previous report.[9] ICG dissolved in 100% CH_3OH was added to the lipid mixture, and then was dried into a thin film. The thin film was rehydrated at 65°C with phosphate-buffered saline (PBS, pH 7.4). Thus, the targeted probes (ICG-liposomes decorated with iRGD [iLPs]) were successfully prepared. Non-targeted probes (ICG-liposomes [LPs]) were prepared using the same method without the addition of DSPE-PEG_{2000}-iRGD. The average diameter and size distribution of iLPs were determined by dynamic light scattering (DLS) (Zetasizer Nano ZS; Malvern Instrument, Malvern, UK). To examine the light exposure stability and imaging performance of targeted probes, samples of free ICG and iLPs containing 10 μg/mL ICG were exposed to overhead fluorescent tube lighting for 24 h, and fluorescent analysis was performed at 0 h, 12 h, and 24 h.

Cellular uptake of targeted probes in vitro

To confirm the targeting performance of iLPs probes, HUVECs (2×10^4 cells/well) were seeded into eight-well chambered cover glasses (Lab-Tek; Nunc, Naperville, IL, USA) with 200 μL of medium, and were incubated with a given amount of TNF-α to simulate the microenvironment of RA. After 24 h, the media were replaced with new media containing LPs or iLPs. The doses of ICG were kept at 10 μg/mL. To test the binding specificity of targeted probes, HUVECs were also pre-blocked by treating with free iRGD for 30 min before adding iLPs. After 3 h of incubation, the cells were washed three times with PBS, followed by fixing with 4% paraformaldehyde for 20 min. After that, the nuclei were stained with 10 μg/mL 4,6-diamidino-2-phenylindole (DAPI) for 5 min and washed thrice with PBS. The fluorescence images were acquired by confocal laser scanning microscope (TCS SP5; Leica Microsystems, Wetzlar, Germany).

Animals and arthritis model

Approval from the Institutional Animal Care and Use Committee of The Third Affiliated Hospital of Southern Medical University was obtained before the study began. First, an intradermal injection of 200 μg of bovine type II collagen emulsified in 200 μg of complete Freund's adjuvant was given to the male DBA/1J mice (8 weeks old; Weitonglihua, Beijing, China) to induce collagen-induced arthritis (CIA). Next, a booster intradermal injection of 100 μg of bovine type II collagen in incomplete Freund's was given to these mice at 21 days after the primary immunization.

Radiographic imaging and NIR fluorescence imaging in vivo

At 2 weeks after secondary immunization, radiographic imaging (X-ray) was performed to assess the joints, thus determining no bone destruction and arthrostenosis in CIA models. Firstly, mice with two symptomatic paws were selected for NIR fluorescence imaging to demonstrate the availability of the imaging modes by iLPs. Mice were intravenously injected with LPs or iLPs, respectively. The equivalent ICG dose was kept at 0.5 mg/kg. The NIR images of mice were obtained at predetermined time points (15 min, 1 h, 3 h, 6 h, 12 h, 24 h) using the ex/in vivo imaging system (Carestream FX Pro; Carestream Health Inc., Toronto, CA, USA) with a 704 nm excitation wavelength and 745 nm filter. Then, mice with one symptomatic paw were selected to demonstrate the accuracy of the imaging modes by iLPs. Then, mice were intravenously injected with iLPs, LPs, or free ICG, respectively. The NIR images of mice were also obtained at predetermined time points (15 min, 2 h) using the ex/in vivo imaging system. At 24 h after injection, the mice were sacrificed and main organs including heart, liver, spleen, lung, and kidney were harvested. Then, main organs were photographed to analyze the biodistribution of iLPs or LPs using the ex/in vivo imaging system. All semi-quantitative data was obtained by Carestream MI software (Carestream Health Inc.).

Histological analysis

To test the sensitivity and accuracy of NIR imaging based on iLPs, and the safety of targeted probes, the mice were sacrificed by anesthesia, and the knee joints and major organs (heart, liver, spleen, lung, and kidney) were harvested, fixed with formalin, and embedded in paraffin. About 7 μm sections were cut with a paraffin slicing machine, followed by staining with hematoxylin-eosin (H&E) dye. To further analyze the relationship between the severity of CIA and fluorescence signal, the immunohistochemical staining of VEGFA and TNF-α was performed.

Statistical analysis

Data are expressed as the mean ± SD. Statistical significance was measured by Student's *t*-test. *P*-values <0.05 were considered significant. SPSS 19.0 software was used for the analysis.

Results

Characterization of targeted probes

iLPs were successfully prepared by thin-film rehydration method (Figure 1A), and the TEM images of iLPs are displayed in Figure 1B. The average diameter of iLPs was measured by DLS, which showed a size of 86.75±0.42 nm (Figure 1C). We next evaluated the fluorescence stability of iLPs. Figure 1D and E indicates that the stability of iLP was superior to that of free ICG ($P<0.01$, Student's *t*-test). The fluorescence intensity of iLPs decreased to 79.6%±4.8% of the initial value after 12 h of light exposure and there was no great decrease until 24 h. In contrast, the fluorescence intensity of free ICG in solution decreased to 15.0%±2.3% of its initial value after 12 h of light exposure and fluorescence signal hardly appeared after 24 h of light exposure.

Cellular uptake of targeted probes in vitro

To investigate the targeted uptake behavior of iLPs, activated HUVECs were incubated with LPs, iLPs, and free ICG. The confocal fluorescence microscopic images are shown in Figure 2, which shows that significantly stronger fluorescence signal is emitted from the cells after incubation with iLPs. But preblocking in the presence of an excess of free iRGD significantly decreased the number of iLPs attached to HUVECs. In addition, it was found that few LPs and free ICG were bound to HUVECs.

The NIR fluorescence imaging in CIA models

CIA models were successfully induced by injection with collagen and Freund's adjuvant, as shown in Figure 3A. By radiographic imaging, it was confirmed that there was no bone destruction and arthrostenosis in the joints with slight clinical manifestations, such as redness and swelling, showing the early manifestations of arthritis (Figure 3B–D). To investigate the effectiveness of NIR imaging by iLPs in CIA models, images were obtained at fixed time intervals after intravenous injection of the targeting probes (Figure 4A). At 15 min after injection, strong fluorescence signal was detected in two swelling paws, and the fluorescence signal in the iLPs group was 3.03-fold higher than that the in LPs group ($P<0.01$, Student's *t*-test). As the time passed, peak

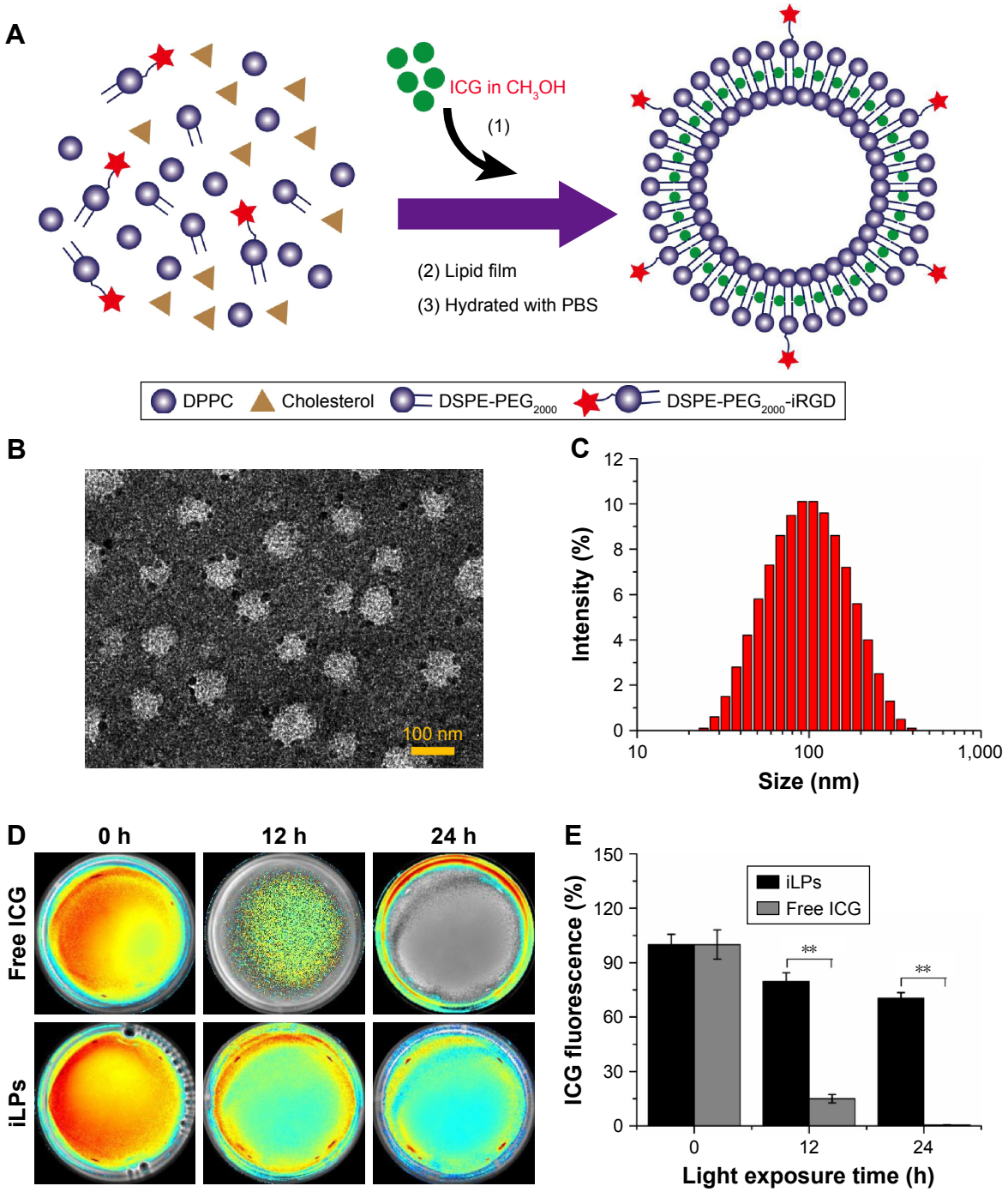

Figure 1 Preparation and characterizaion of iLPs. (**A**) Systemic illustration of preparation of iLPs. (**B**) Morphology of iLPs by TEM. (**C**) Size distrubition of iLPs. (**D**) Fluorescence image of iLPs and free ICG after light exposure. (**E**) Quantitative analysis of fluorescence intensity of iLPs and free ICG after light exposure, the stability of iLP was found to be superior to that of free ICG (**$P<0.01$).

Abbreviations: iLPs, ICG-liposomes decorated with iRGD; TEM, transmission electron microscopy; ICG, indocyanine green; DPPC, dipalmitoylphosphatidylcholine; DSPE-PEG_{2000}, 1,2-distearoyl-sn-glycero-3-pho-sphoethanolamine-N-[met-hoxy(poly-ethyleneglycol)-2000]; iRGD, targeting peptide (CRGDKGPDC).

fluorescence signals were observed at 6 h after administration of iLPs, and the signal intensity in iLPs was 4.25-fold higher than in LPs, and the original low fluorescence signals in the LPs group had decreased at 3 h after injection. Within 24 h, the fluorescence signals in iLPs group was always higher than that in LPs group, thus indicating that the NIR fluorescence imaging by iLPs possessed high sensitivity and stability (Figure 4B).

To demonstrate the accuracy of the imaging modes by iLPs, mice with one symptomatic paw were selected and the photos were attained at fixed time points by NIR imaging. At 15 min after injection, the fluorescence signal from

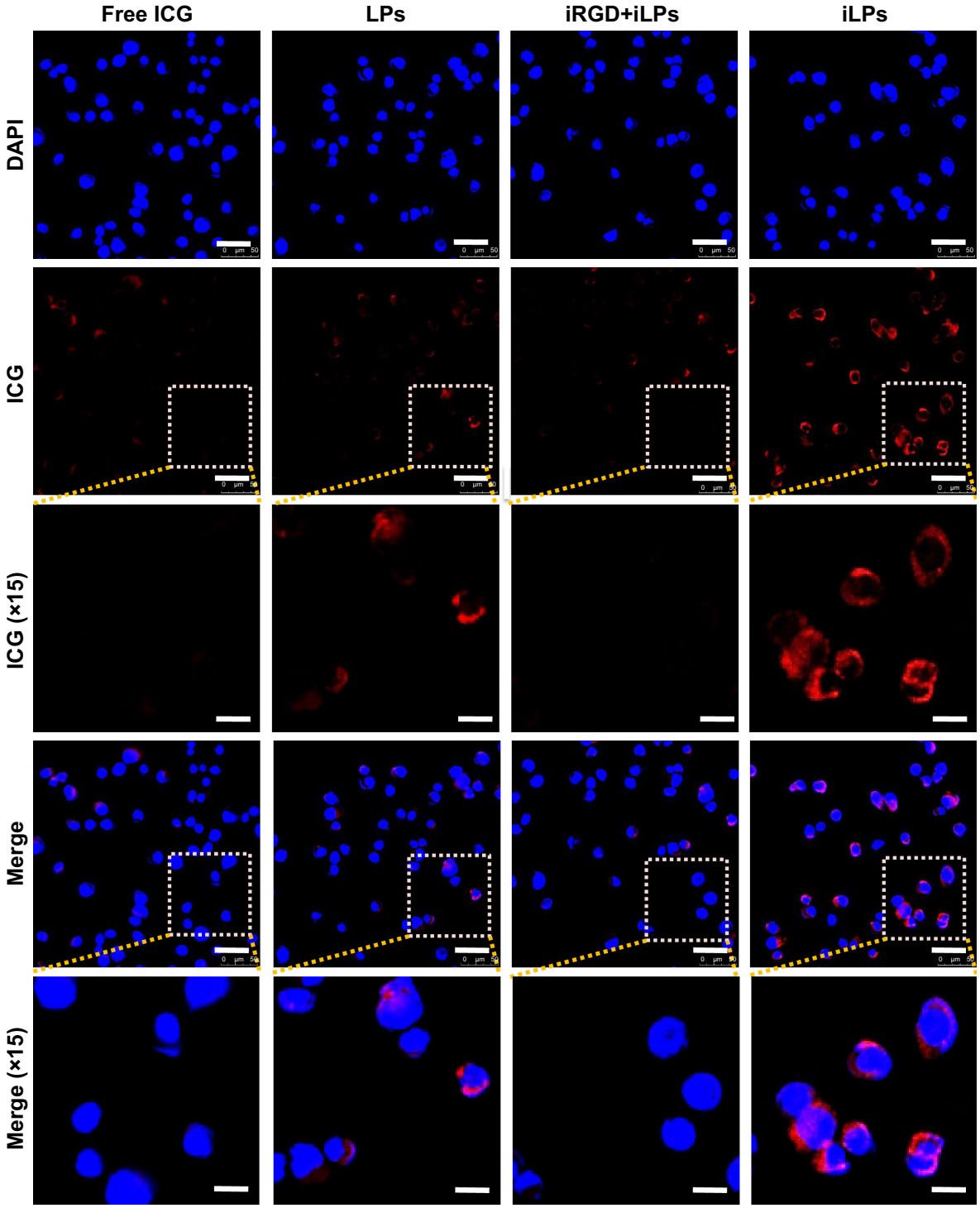

Figure 2 Targeted cellular uptake of iLPs. Confocal fluorescence images displayed cellular uptake of ICG after incubation with free ICG, LPs, iRGD+iLPs, or iLPs. Blue represents the localization of cell nucleus with the fluorescence of DAPI and red represents the localization of ICG (scale bar, 50 μm).
Abbreviations: iLPs, ICG-liposomes decorated with iRGD; LPs, ICG-liposomes; ICG, indocyanine green; iRGD, targeting peptide (CRGDKGPDC).

iLPs was localized selectively in inflamed paws, whereas the signal could almost not be observed in the non-inflamed paws, thus showing high accuracy for iLPs (Figure 4C). For LPs and free ICG, the fluorescence signal in the inflamed paws was far weaker than for iLPs. At 2 h after injection, the accumulation of iLPs in the inflamed paws did not show a great change, almost achieving the peak of the fluorescence signal. Notably, the signal of free ICG in the inflamed joints had dispersed after 2 h, and the false positive results can be seen in non-inflamed paws of LPs group.

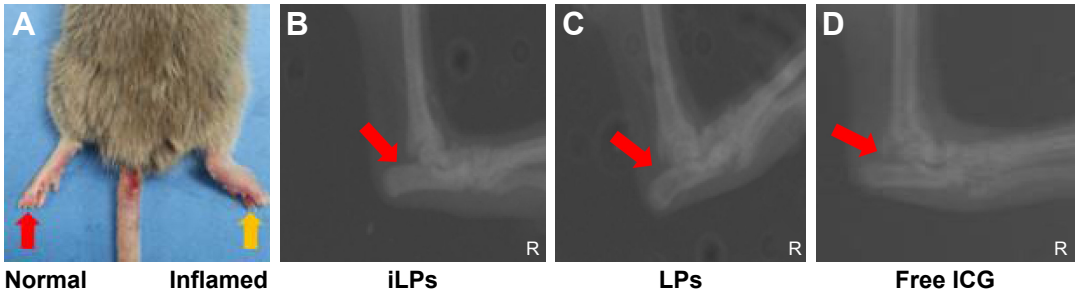

Figure 3 RA model and radiological evalution. (**A**) RA models were successfully induced by injection with collagen and Freund's adjuvant. (**B**, **C**, and **D**) Radiological evaluation showed there was no joint destruction and interarticular stenosis in inflamed paw in mice pretreated with iLPs, LPs, and free ICG. The yellow arrow indicates the normal paw, and the red arrow indicate the inflamed paw.
Abbreviations: iLPs, ICG-liposomes decorated with iRGD; LPs, ICG-liposomes; ICG, indocyanine green; RA, rheumatoid arthritis; iRGD, targeting peptide (CRGDKGPDC).

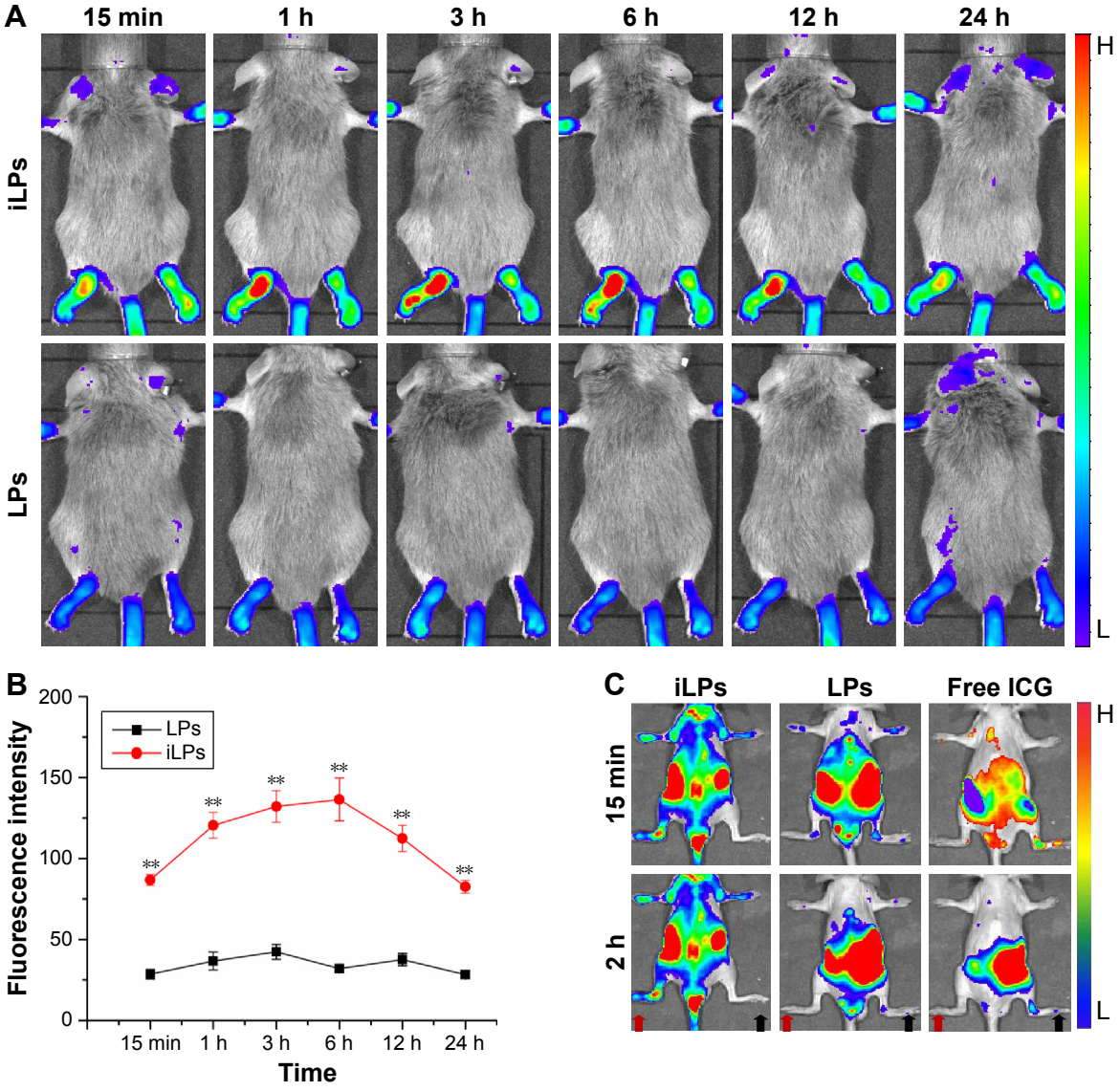

Figure 4 NIR fluorescence imaging in RA models. (**A**) NIR imaging of RA models with two symptomatic paws was performed at predetermined times after injection with iLPs and LPs, and stronger fluorescence signal in was detected in iLPs group than in LPs group, achieving high sensitivity for NIR fluorescence imaging by iLPs. (**B**) The semi-quantitative analysis of NIR fluorescence imaging in RA models with two symptomatic paws displayed that the fluorescence signal was always higher in iLPs group than in LPs group within 24 h (**$P<0.01$). (**C**) NIR imaging of RA models with one inflamed paw was performed at predetermined time intervals (15 min, 2 h) after injection with iLPs, LPs, or free ICG, and strong fluorescence signal was detected in inflamed joint (red arrow) and almost no signal was detected in normal joint (black arrow) in iLPs group, achieving high specificity for NIR fluorescence imaging by iLPs.
Abbreviations: iLPs, ICG-liposomes decorated with iRGD; LPs, ICG-liposomes; ICG, indocyanine green; iRGD, targeting peptide (CRGDKGPDC); RA, rheumatoid arthritis; NIR, near-infrared.

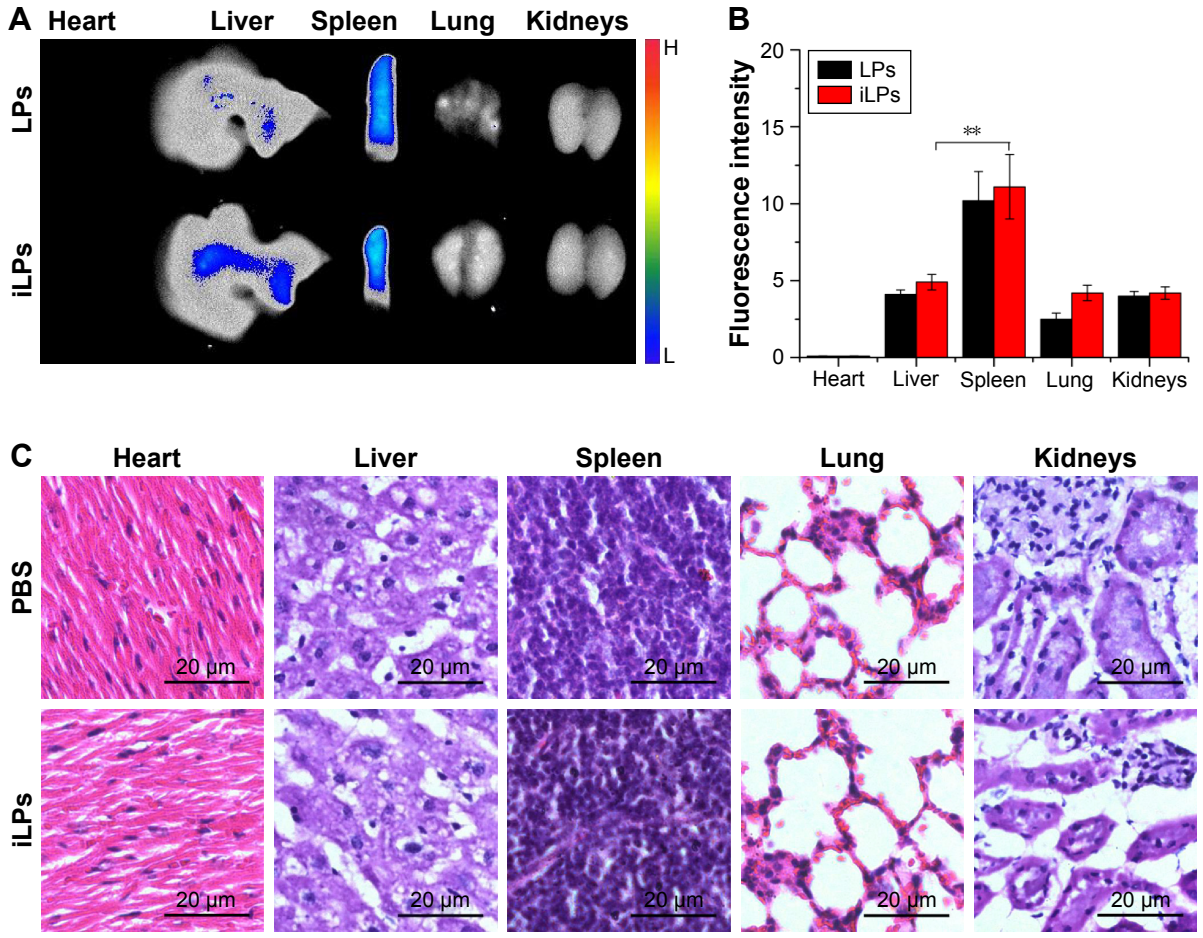

Figure 5 The biodistribution and safety analysis in main organs. (**A**) Biodistribution of iLPs and LPs in the main organs at 24 h after injection. (**B**) The semi-quantitative analysis for biodistribution of iLPs and LPs; there was no significant difference in the same organs ($P>0.05$), but the fluorescence signals in spleen was a little higher than in liver (**$P<0.01$), which is different from the previous studies which were conducted in tumor models. (**C**) H&E stained images of major organ slices collected from normal DAB/1J mice and RA models treated with iLPs; no significant difference was observed, showing that iLPs had a favorable safety profile.

Abbreviations: H&E, hematoxylin-eosin; iLPs, ICG-liposomes decorated with iRGD; LPs, ICG-liposomes; ICG, indocyanine green; iRGD, targeting peptide (CRGDKGPDC); RA, rheumatoid arthritis.

The biodistribution of targeted probes and safety in main organs

At 24 h after injection of targeted probes, the biodistribution of targeted probes was analyzed (Figure 5A). The semi-quantitative analysis of fluorescence intensities of ex vivo organs showed that the fluorescence signals were mainly detected in liver and spleen (Figure 5B). For iLPs and LPs, there was no significant difference in the signal within the same organs ($P>0.05$, Student's *t*-test), but the fluorescence signals in spleen was a little higher than that in liver ($P<0.01$, Student's *t*-test), which is in contrast to the results reported by the previous studies that were conducted in tumor models. When the safety of targeted probes was evaluated, histological analysis of the main organs from mice treated with iLPs did not find any appreciable abnormality when compared with the organs from normal mouse (Figure 5C). To some extent, iLPs were tolerable and showed no obvious acute toxicity in the examined mice.

Histological analysis

To further investigate the accuracy of NIR imaging, tissue sections of inflamed and non-inflamed joints were examined by H&E staining and immunohistochemical staining of VEGFA and TNF-α. Figure 6A and B displays images of inflamed and non-inflamed joints and synovium. The results indicated that inflamed paws showed only slight synovial hypertrophy with no bone destruction as well as overexpression of VEGFA and TNF-α. The results are similar to those obtained by NIR imaging of iLPs.

Discussion

Early diagnosis and effective monitoring of RA are important for a favorable prognosis. Moreover, medical imaging, as an indispensable tool, has become the mainstay of diagnosis and treatment monitoring for RA.[3] Early studies mainly focused on conventional radiography, which allows the visualization of anatomical changes in established RA, such as joint space

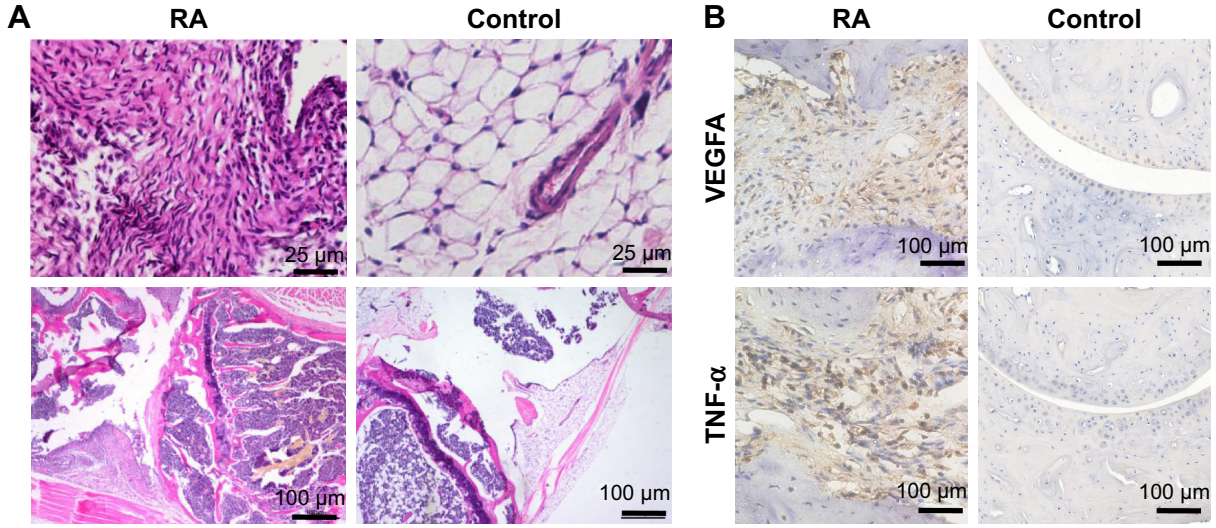

Figure 6 Histological analysis. (**A**) H&E staining shows hyperplastic synovium in inflamed joint and non-hyperplastic synovium in normal joint, which matched the results of NIR fluorescence imaging, further confirming the high specificity of imaging modes. (**B**) The immunohistochemical staining indicated the overexpression of VEGFA and TNF-α in inflamed joint, which showed that imaging by using iLPs as probes can reflect the severity of RA, to some extent.
Abbreviations: RA, rheumatoid arthritis; NIR, near-infrared.

narrowing, erosions, and juxta-articular bone loss.[4] Subsequent studies suggested that MRI can detect not only synovial hyperplasia, cartilage degradation, and bone changes but also signs of RA in the pre-erosive phase.[5,7] While most of these studies have greatly improved in anatomical imaging of established RA, recent studies found that optical fluorescence imaging based on fluorescence probes can provide more meaningful information in early RA.[16–21]

In our current study, we found that αvβ3-targeted in vivo fluorescence imaging in CIA models is a sensitive, specific, and quantifiable molecular imaging technique. These findings were consistent with those reported by other studies that used targeted fluorescence probes to overcome the limitations in the diagnosis of early RA.[22–24] For example, Gompels et al reported that the mean fluorescence intensity measured in CIA models demonstrated a 2.34-fold increase in inflamed paws at 8 hours following injection of NIR fluorescence–labeled E-selectin antibody, as compared to that in the control antibody.[23] Yet, our results go well beyond these findings as we achieved the primary goal of demonstrating that the mean fluorescence signal measured in CIA models obtained a 3.03-fold increase in inflamed paws at 15 min following injection of iLPs when compared with LPs. In addition, the peak fluorescence signal in iLPs was 4.25-fold higher than that in LPs at 6 h after injection, thus indicating favorable availability of iLPs. Taken together, this is thought to occur due to the introduction of iRGD peptides, which can specifically bind to the integrin αvβ3 receptor which is overexpressed in angiogenesis.[25,26] With regard to in vitro cellular uptake, iLPs showed a favorable targeted ability compared to LPs. Moreover, studies demonstrated that angiogenesis is an early event in the inflammatory joint that is fundamental for enabling activated monocytes to enter the synovium and expand it into a pannus via ECs by active recruitment, resulting in cartilage degradation and bone destruction.[12–14] Furthermore, studies also showed that ECs lining the synovial blood vessels express integrins, such as αvβ3, early in blood vessel formation, and later express adhesion molecules (eg, E-selection) and ki-67, which are markers of EC adhesion and proliferation.[27,28] Therefore, for an early RA diagnosis, fluorescence imaging based on integrin αvβ3, to some extent, was superior to that based on anti-E-selectin NIR fluorescence probes and protease-activated NIR fluorescence probes (proteases are produced by macrophages via synovial blood vessels by active recruitment).

While these results are exciting in achieving the primary goal of using iLPs to achieve sensitive NIR fluorescence imaging, it must be acknowledged that favorable specificity was also essential for the diagnosis of early arthritis. Along these lines, mice with one symptomatic paw were selected and the photos were obtained at fixed time points by NIR fluorescence imaging. At 15 min after injection, the fluorescence signal from iLPs localized selectively in the inflamed paws, whereas the signal can almost not be observed in the non-inflamed paws. These results were further confirmed by H&E staining and immunohistochemical staining of VEGFA

and TNF-α. Histological analysis displayed that the paws with strong fluorescence signal showed slight synovial hyperplasia and new vessels, and the paws with no fluorescence signal were confirmed to be the normal joint, further showing high accuracy of iLPs. For the groups injected with LPs and free ICG, the fluorescence signal in the inflamed paws was stronger in the LPs group than that in the free ICG group. The phenomenon may be interpreted by the following reasons. Firstly, ICG entrapped in liposomes can avoid binding to plasma proteins after intravenous injection, followed by rapid liver elimination and bile excretion pathway, and increase the amount of ICG monomer, thus improving the stability of ICG.[29] Additionally, dysfunctional vessels in RA, like tumor vessels, increased the leakiness and permeability of vessels, which enhanced the LPs accumulation in inflamed joints by enhanced permeability and retention (EPR).[10] Similar phenomenon was also reported where ICG-lactosome fluorescence in inflamed paws was higher than free ICG in inflamed paws. But the initial time and peak time of fluorescence signal in ICG-lactosomes occur much later than those in LPs, which may be attributed to the ability of cells to internalize liposomes more rapidly over that to internalize lactosomes.[30,31] Taken together, the above mentioned findings further explain the reason for rapid aggregation of iLPs in the inflamed paws within just 15 min.

Compared with the availability of targeted probes, the biodistribution of probes was equally important, which is closely related to biosafety and validity. With regard to biodistribution, the accumulation of iLPs or LPs in spleen was found to be a little higher than in liver through ex vivo NIR imaging, which was different compared to the previous reports in tumors showing that the accumulation of nanoparticles in liver was much more than that in spleen. This slight difference may originate from the CIA models and the size of nanoparticles. The CIA models were induced by immunization in DAB/1J mice, but not in Babl/C mice or C57 mice, which are tumor models. Studies also demonstrated that the volume of spleen in CIA models was much larger than in normal mice,[32] which may facilitate phagocyte migration to spleen. In addition, nanoparticles of size less than 200 nm can remain in circulation for a longer period of time and can easily be swallowed by the spleen due to their rich blood supply and the abundance of tissue-resident phagocytes.[33]

Although the NIR fluorescence imaging method based on iLPs has some advantages, we acknowledge several limitations in our study. Firstly, although the CIA mice used in many studies is a well characterized RA model, the CIA models can not completely reflect RA. Additionally, the early RA was evaluated only according to radiological imaging, which may not be sufficiently accurate. We controlled the time course of induction, making them keep in the early stage of disease as soon as possible.

Conclusion

Noninvasive NIR fluorescence imaging using iRGD-targeted liposomes as fluorescence probes may facilitate improved arthritis diagnosis and early assessment of the disease progression by providing an in vivo characterization of angiogenesis in inflammatory joint diseases. In the future, it could certainly offer more potential clinical benefits, including a suitable therapy choice, therapy dosing, quantitative early evaluation of clinical outcome, and more effective drug development.

Acknowledgments

The authors gratefully acknowledge the support received for this research from National Key Basic Research Program of China (973 Program) (Grant Nos 2015CB755500, 2014CB744502, 2013CB733800), National Natural Science Foundation of China (Grant Nos 81371563, 81360482, 11325420, 81401435, 81571674, 81771853, 61327001), Natural Science Foundation of Guangdong Province (Grant No 2014A030313341), Scientific Technology Foundation of Guangdong Province (Grant No 2014A020212169), and Guangzhou Science and Technology Program Project (Grant No 201607010115).

Disclosure

The authors report no conflicts of interest in this work.

References

1. Feldmann M, Brennan FM, Maini RN. Rheumatoid arthritis. *Cell*. 1996; 85(3):307–310.
2. Finckh A, Liang MH, van Herckenrode CM, de Pablo P. Long-term impact of early treatment on radiographic progression in rheumatoid arthritis: a meta-analysis. *Arthritis Rheum*. 2006;55(6):864–872.
3. Zeman MN, Scott PJ. Current imaging strategies in rheumatoid arthritis. *Am J Nucl Med Mol Imaging*. 2012;2(2):174–220.
4. Guillemin F, Billot L, Boini S, Gerard N, Odegaard S, Kvien TK. Reproducibility and sensitivity to change of 5 methods for scoring hand radiographic damage in patients with rheumatoid arthritis. *J Rheumatol*. 2005;32(5):778–786.
5. Klarlund M, Ostergaard M, Jensen KE, Madsen JL, Skjodt H, Lorenzen I. Magnetic resonance imaging, radiography, and scintigraphy of the finger joints: one year follow up of patients with early arthritis. The TIRA Group. *Ann Rheum Dis*. 2000;59(7):521–528.
6. Szkudlarek M, Narvestad E, Klarlund M, Court-Payen M, Thomsen HS, Ostergaard M. Ultrasonography of the metatarsophalangeal joints in rheumatoid arthritis: comparison with magnetic resonance imaging, conventional radiography, and clinical examination. *Arthritis Rheum*. 2004;50(7):2103–2112.

7. Boyesen P, Haavardsholm EA, van der Heijde D, et al. Prediction of MRI erosive progression: a comparison of modern imaging modalities in early rheumatoid arthritis patients. *Ann Rheum Dis*. 2011;70(1):176–179.
8. Zhao PF, Zheng MB, Yue CX, et al. Improving drug accumulation and photothermal efficacy in tumor depending on size of ICG loaded lipid-polymer nanoparticles. *Biomaterials*. 2014;35(23):6037–6046.
9. Yan F, Wu H, Liu H, et al. Molecular imaging-guided photothermal/photodynamic therapy against tumor by iRGD-modified indocyanine green nanoparticles. *J Control Release*. 2016;224:217–228.
10. Kennedy A, Ng CT, Biniecka M, et al. Angiogenesis and blood vessel stability in inflammatory arthritis. *Arthritis Rheum*. 2010;62(3):711–721.
11. Firestein GS. Starving the synovium: angiogenesis and inflammation in rheumatoid arthritis. *J Clin Invest*. 1999;103(1):3–4.
12. Koch AE. Angiogenesis as a target in rheumatoid arthritis. *Ann Rheum Dis*. 2003;62(Suppl 2):ii60–ii67.
13. Szekanecz Z, Koch AE. Angiogenesis and its targeting in rheumatoid arthritis. *Vasc Pharmacol*. 2009;51(1):1–7.
14. Vervoordel-Donk M, van Holten J, Adriaansen J, Bevaart L, Tak PP. Inhibition of angiogenesis by interferon-beta protein and gene therapy in animal models of arthritis and rheumatoid arthritis (RA) patients: implications for targeting vascularity in RA. *Arthritis Rheum*. 2008;58(9):S660–S.
15. Storgard CM, Stupack DG, Jonczyk A, Goodman SL, Fox RI, Cheresh DA. Decreased angiogenesis and arthritic disease in rabbits treated with an alphavbeta3 antagonist. *J Clin Invest*. 1999;103(1):47–54.
16. Mountz J, Alavi A, Mountz J. Emerging optical and nuclear medicine imaging methods in rheumatoid arthritis. *Nat Rev Rheumatol*. 2012;8(12):719–728.
17. Schäfer VS, Hartung W, Hoffstetter P, et al. Quantitative assessment of synovitis in patients with rheumatoid arthritis using fluorescence optical imaging. *Arthritis Res Ther*. 2013;15(5):R124.
18. Chan MM, Gray BD, Pak KY, Fong D. Non-invasive in vivo imaging of arthritis in a collagen-induced murine model with phosphatidylserine-binding near-infrared (NIR) dye. *Arthritis Res Ther*. 2015;17(1):50.
19. Werner SG, Langer HE, Schott P, et al. Indocyanine green-enhanced fluorescence optical imaging in patients with early and very early arthritis: a comparative study with magnetic resonance imaging. *Arthritis Rheum*. 2013;65(12):3036–3044.
20. Werner SG, Langer HE, Ohrndorf S, et al. Inflammation assessment in patients with arthritis using a novel in vivo fluorescence optical imaging technology. *Ann Rheum Dis*. 2012;71(4):504–510.
21. Meier R, Thuermel K, Noël PB, et al. Synovitis in patients with early inflammatory arthritis monitored with quantitative analysis of dynamic contrast-enhanced optical imaging and MR imaging. *Radiology*. 2014;270(1):176–185.
22. Chen W-T, Mahmood U, Weissleder R, Tung C-H. Arthritis imaging using a near-infrared fluorescence folate-targeted probe. *Arthritis Res Ther*. 2005;7(2):R310.
23. Gompels LL, Madden L, Lim NH, et al. In vivo fluorescence imaging of E-selectin: quantitative detection of endothelial activation in a mouse model of arthritis. *Arthritis Rheum*. 2011;63(1):107–117.
24. Wunder A, Tung CH, Muller-Ladner U, Weissleder R, Mahmood U. In vivo imaging of protease activity in arthritis: a novel approach for monitoring treatment response. *Arthritis Rheum*. 2004;50(8):2459–2465.
25. Sugahara KN, Teesalu T, Karmali PP, et al. Coadministration of a tumor-penetrating peptide enhances the efficacy of cancer drugs. *Science*. 2010;328(5981):1031–1035.
26. Sugahara KN, Teesalu T, Karmali PP, et al. Tissue-penetrating delivery of compounds and nanoparticles into tumors. *Cancer Cell*. 2009;16(6):510–520.
27. Khong TL, Larsen H, Raatz Y, Paleolog E. Angiogenesis as a therapeutic target in arthritis: learning the lessons of the colorectal cancer experience. *Angiogenesis*. 2007;10(4):243–258.
28. Walsh DA, Wade M, Mapp PI, Blake DR. Focally regulated endothelial proliferation and cell death in human synovium. *Am J Pathol*. 1998;152(3):691–702.
29. Zheng X, Zhou F, Wu B, Chen WR, Xing D. Enhanced tumor treatment using biofunctional indocyanine green-containing nanostructure by intratumoral or intravenous injection. *Mol Pharm*. 2012;9(3):514–522.
30. Akahoshi A, Matsuura E, Ozeki E, Matsui H, Watanabe K, Ohtsuki T. Enhanced cellular uptake of lactosomes using cell-penetrating peptides. *Sci Technol Adv Mater*. 2016;17(1):245–252.
31. Onishi S, Sakane M, Tsukanishi T, et al. Near-infrared fluorescence imaging with indocyanine green-lactosomes in a mouse model of rheumatoid arthritis. *Mod Rheumatol*. 2016;26(6):885–890.
32. Han Y, Li X, Zhou Q, et al. FTY720 abrogates collagen-induced arthritis by hindering dendritic cell migration to local lymph nodes. *J Immunol*. 2015;195(9):4126–4135.
33. Maruyama K. Intracellular targeting delivery of liposomal drugs to solid tumors based on EPR effects. *Adv Drug Deliv Rev*. 2011;63(3):161–169.